Triple Junction Mobility: A Molecular Dynamics Study

MONEESH UPMANYU

Department of Materials Science and Engineering, University of Michigan, Ann Arbor, MI 48109, USA; and Department of Mechanical and Aerospace Engineering, Princeton University, Princeton, NJ 08544, USA

molu@umich.edu; molu@engin.umich.edu

D.J. SROLOVITZ

Department of Mechanical and Aerospace Engineering, Princeton University, Princeton, NJ 08544, USA; and Princeton Materials Institute, Princeton University, Princeton, NJ 08544, USA

srol@princeton.edu

L.S. SHVINDLERMAN

Institute of Solid State Physics, Russian Academy of Sciences, Chernogolovka, Moscow distr. 142432, Russia; and Institut für Metallkunde und Metallphysik, RWTH Aachen, D-52056 Aachen, Germany

G. GOTTSTEIN

Institut für Metallkunde und Metallphysik, RWTH Aachen, D-52056 Aachen, Germany

Abstract. We present a molecular dynamics simulation study of the migration of individual grain boundary triple junctions. The simulation cell was designed to achieve steady state migration. Observations of the triple junction angle and grain boundary profiles confirm that steady state was achieved. The static, equilibrium grain boundary triple junction angles and the dynamic triple junction angles were measured as a function of grain size and grain boundary misorientation. In most cases, the static and dynamic triple junction angles are nearly identical, while substantial deviations were observed for low Σ boundary misorientations. The intrinsic, steady-state triple junction mobilities were extracted from measurements of the rate of change of grain boundary area in simulations with and without triple junctions. The triple junction velocity is found to be inversely proportional to the grain size width. The normalized triple junction mobility exhibits strong variations with boundary misorientation, with strong minima at misorientations corresponding to orientations corresponding to low values of Σ. The triple junctions create substantial drag on grain boundary migration at these low mobility misorientations.

Keywords: triple junction mobility, thermodynamic equilibrium, grain boundary energy, grain boundary migration, static and dynamic triple junction angles, steady-state triple junction migration, special (high coincidence) boundaries, triple junction drag

I. Introduction

If we view grain boundaries as the two-dimensional surfaces separating grains of different orientations, then triple junctions are naturally described as the linear defects at which three grain boundaries meet. Just as grain boundaries, dislocations, vacancies, and in-terstitials are part of the pantheon of crystal defects with distinct properties, triple junctions also possess unique characteristics. Triple junctions are known to be short circuit diffusion paths [1, 2]; commonly exhibiting higher diffusivities than grain boundaries. They serve as preferential sites for the nucleation of cavities and cracks during superplasticity and creep [3].

Corrosion may preferentially occur at triple junctions [4]. Triple junctions play an important role in certain classes of plastic deformation, e.g. they resist grain boundary sliding, resulting in localized deformation zones or grain boundary folding [5]. The structure and thermodynamic properties of triple junctions have only recently garnered the attention of the research community. The atomic structure of triple junctions may be elucidated, in part, by consideration of the structure of the grain boundaries that meet there. Associated with this atomic structure is a well defined strain field and a core, with an associated core energy [6]. Recent atomistic simulations suggest that, in certain cases, the triple junction energy can be negative [7].

Classical theories of grain growth are based on the constancy (i.e., time, velocity, grain size independence) of the triple junction (dihedral) angles (where three grain boundaries meet). These angles are usually viewed as the thermodynamic dihedral angles where the constituent grain boundary surface tensions are balanced (i.e., Young's angles). Knowledge of the Young's angles at the triple junctions bounding a grain boundary provides a means for determining the integral of the boundary curvature, which is a central variable in grain growth theories (see e.g., [8]). In two-dimensions, where topology is relatively simple, this gives rise to the famous $(n - 6)$ rule for grain growth, which states that grains with more than six sides $(n > 6)$ grow, while those with fewer sides shrink [8].

Importantly, in order for Young's angles to remain fixed as the constituent grain boundaries migrate, the triple junction mobility must be infinite. The assumed infinite mobility of the triple junctions can be understood by considering the motion of grain boundaries. The relationship between boundary velocity, v_b, and driving force, F_b, is commonly written as

$$v_b = M_b F_b, \qquad (1)$$

where M_b is the intrinsic grain boundary mobility. This relationship arises from the assertion that grain boundary motion is dissipative. For the specific cases where curvature is the primary driving force (as in grain growth), the driving force is proportional to the grain boundary curvature, and Eq. (1) becomes

$$v_b = M_b \gamma \kappa, \qquad (2)$$

where γ and κ are the grain boundary energy and curvature, respectively. Because the grain boundary curvature is singular at the triple junction, Eq. (2) suggests that any deviations from Young's angles are restored

with infinite velocity. Therefore, Young's angle should always be fixed at the triple junction and, hence, it is usually viewed as providing a boundary condition on the slopes of the grain boundaries meeting at the triple junction. Assuming that the migration of triple junctions is dissipative, the triple junction migration rate v_{TJ} can be written as

$$v_{TJ} = M_{TJ} F_{TJ}, \qquad (3)$$

where M_{TJ} is the intrinsic triple junction mobility due to a driving force F_{TJ}. Preservation of the Young's angles during boundary migration implies that the grain boundary energies are balanced at the triple junction, and that the driving force F_{TJ} is zero. Hence, a finite triple junction migration rate is possible only if the triple junction mobility is M_{TJ} infinite. Since deviations from Young's angles are restored infinitely fast, it is safe to assume that the triple junction mobility is infinite throughout its migration and does not affect the migration of the associated grain boundaries.

A counter to the assertion that triple junctions have infinite mobility arises if one views triple junctions not as mathematical lines (in 3-d) but as defects with a well-defined atomic structure constrained by the crystallography imposed by its constituent grain boundaries. As such, triple junction motion must involve atomic rearrangement over finite distances and times and, hence, be dissipative—as assumed above by the form of Eq. (3). Since triple junctions have atomic structure distinct from those of its constituent grain boundaries, a distinct, finite, intrinsic triple junction mobility seems plausible. Does that in turn imply that the (dynamic) angles of moving grain boundary triple junctions are different from the static equilibrium angles? If so, then how do this finite mobility and the dynamic angles depend on the grain boundary structure? How does the intrinsic triple junction mobility compare with that of its constituent grain boundaries? These questions form the basis of the present study.

Recently, several studies have examined the role of triple junctions in the evolution of polycrystalline structures—particular in relation to grain growth and recrystallization. King [6] have performed a detailed study of the structure of symmetrical triple junctions and the parameters on which the stability of these junctions depend. The unrelaxed atomic structure of these junctions has also been studied by superposition of three, rotated three dimensional lattices [9] or by matching two dimensional structures which arise in grain boundaries [10]. Experimental and theoretical studies by Galina et al. [11, 12] focussed on

determining the conditions under which triple junction mobility affects grain boundary migration. Lazarenko et al. [13] examined the grain boundary orientations in the vicinity of triple junction in the early stages of recrystallization of tungsten. Interestingly, they found that in the deformed state, the triple junction angle distribution showed peaks at $\pi/2$, $2\pi/3$ and π. However, annealing the sample reduced the angular dispersion to a single peak centered around the expected $2\pi/3$ value. These experiments show that the triple junctions play a complicated role in the structure and dynamics of the polycrystalline state.

In this paper, we present results from molecular dynamics simulations of triple junction migration as a function of grain size and misorientation. We first outline the theory behind the simulation approach and then describe the simulation geometry used to study steady-state migration of triple junctions. We report dynamic and static Young's angle measurements and mobilities for thirteen different triple junction misorientations. The triple junction data is analyzed by comparing it with grain boundary mobility data extracted in a previous simulation study. The implication of the extracted triple junction mobilities for the evolution of polycrystalline structures are discussed.

II.   Theoretical and Experimental Background

In this study, we are primarily interested in determining whether the intrinsic triple junction mobility is finite, and if so, determine its magnitude. In order to put these results into perspective, the magnitude of the triple junction mobility should be related to the intrinsic grain boundary and triple junction variables, such as the intrinsic grain boundary mobilities and energies, and the (dynamic and static) triple junction Young's angles, etc. The present simulations focus on triple junction motion driven by the curvature of the boundaries that meet at the triple junction. This choice was made because grain boundary curvature is the primary driving force that governs the kinetics of grain growth. The methodology employed is designed to extract the triple junction mobility in the *steady-state* regime, where the triple junction migrates at fixed rate with a self-similar geometry. Finally, in order to parameterize and compare the triple junction mobility with that of its constituent grain boundaries, the tricrystallography was chosen such that the mobilities of the constituent grain boundaries were known from previous simulations.

Figure 1(a) is a schematic illustration of the triple junction migration geometry used in the present study.

Three grains a, b_1 and b_2 separated by three grain boundaries with misorientations θ_{ab_1}, θ_{ab_2} and $\theta_{b_1b_2} = \theta_{ab_1} + \theta_{ab_2}$ (only one variable is required to describe misorientation in 2-d) meet at the triple junction. The static force balance at the triple junction associated with the individual grain boundary energies results in a thermodynamic driving force, $F_{TJ(s)}$, given by,

$$F_{TJ(s)} = \gamma_{ab_1} \cos \beta_{ab_1} + \gamma_{ab_2} \cos \beta_{ab_2} - \gamma_{b_1b_2}, \quad (4)$$

where γ_{ab_1}, $\gamma_{b_1b_2}$ and γ_{ab_2} are the grain boundary energies and β_{ab_1}, and β_{ab_2} are the included angles within grain a. When the symmetry condition $\theta_{ab_1} = \theta_{ab_2} = \theta$ ($=\theta_{b_1b_2}/2$) is imposed, the grain boundaries ab_1 and ab_2 are equivalent, $\gamma_{ab_1} = \gamma_{ab_2} = \gamma$ and $\beta_{ab_1} = \beta_{ab_2} = \beta_s$, (henceforth referred to as the static triple junction (Young's) angle). Static equilibrium is achieved when, $F_{TJ(s)} = 0$; implying the following relationship between β_s and the grain boundary energies

$$2\gamma \cos \beta_s = \gamma_{b_1b_2}. \quad (5)$$

The driving force, $F_{TJ(d)}$, which results in triple junction migration, can be determined from a force balance in terms of the dynamic triple junction angle β_d. This formulation assumes the dynamic triple junction angle β_d can be different from the equilibrium (static) triple junction angle β_s. Using Eq. (5) for the symmetrical grain boundaries case, we obtain

$$F_{TJ(d)} = 2\gamma \cos \beta_d - \gamma_{b_1b_2}$$
$$= 2\gamma (\cos \beta_d - \cos \beta_s). \quad (6)$$

Hence, a non-zero driving force in the dynamic case implies that the dynamic angle β_d is different from the static triple junction angle β_s. Assuming that triple junction migration is dissipative, Eqs. (3) and (6) allow us to express the overall triple junction migration rate v_{TJ} as

$$v_{TJ} = M_{TJ} F_{TJ(d)} = 2\gamma M_{TJ}(\cos \beta_d - \cos \beta_s). \quad (7)$$

We can easily extract the triple junction migration rate in terms of a quantity which can be extracted from the simulations as well as experiments, i.e. the rate of change of area $\dot{A}_{TJ}$ of the half-loop grain a (see Fig. 1(a)). $\dot{A}_{TJ}$ is simply the product of the width of grain a, w, and the triple junction velocity, v_{TJ}. If v_{TJ} is constant (see Eq. (7)), $\dot{A}_{TJ}$ is constant:

$$\dot{A}_{TJ} = v_{TJ}w = 2 M_{TJ}\gamma (\cos \beta_d - \cos \beta_s)w. \quad (8)$$
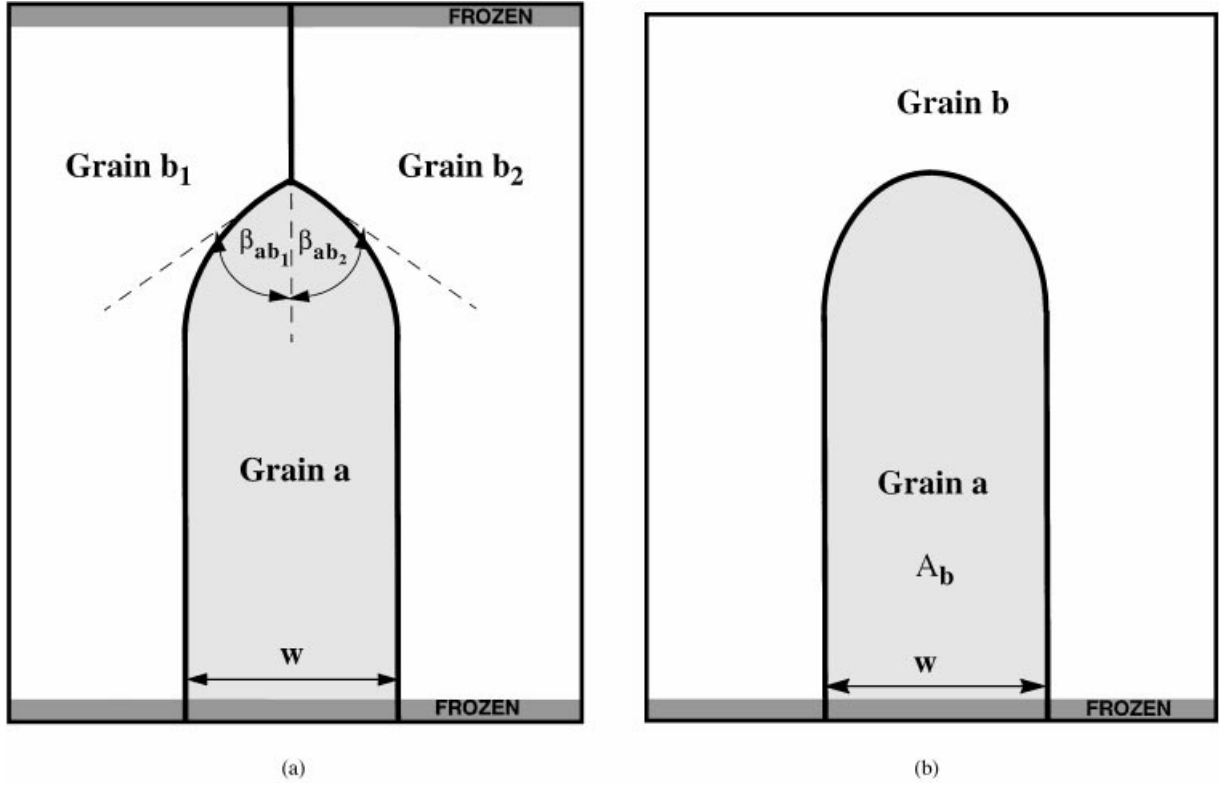
Figure 1. (a) A schematic illustration of the simulation cell geometry for a system containing a triple junction formed by a half-loop grain a (width w and area A_{TJ}). The misorientation across the ab_1 and across the ab_2 boundaries is θ and that across the b_1b_2 boundary is 2θ. The bottom three atomic planes of the simulation cell are frozen to maintain the desired misorientations, while the top three atomic planes are frozen in the X-direction only, and allowed to move in the Y-direction. The remaining atoms are thermostated at the desired temperature. All of the remaining surfaces are free. (b) Same as in (a) but for a bicrystal half-loop of width w and area A_b. In this case, only the bottom 3 layers are frozen and the remaining surfaces are free.

In the simulations, we fix w and measure $\dot{A}_{TJ}$, β_d and β_s in order to extract the reduced mobility $M_{TJ}\,\gamma$ of the triple junction, as per Eq. (8). The steady-state migration velocity of the triple junction in the geometry indicated in Fig. 1(a) was determined analytically by Galina et al. under the assumption of motion by mean curvature, constant β_d and $\theta_{ab_1} = -\theta_{ab_2} = \theta$. They found [11]

$$v_{TJ} = \frac{2\beta_d M_b \gamma}{w}. \qquad (9)$$

implying that

$$\dot{A}_{TJ} = v_{TJ}w = 2\beta_d M_b \gamma, \qquad (10)$$

where M_b is the mobility of the ab grain boundaries. Determination of $\dot{A}_{TJ}$ from Eq. (10) requires an independent measurement of the intrinsic reduced

boundary mobility $M_b\gamma$ under the same conditions (misorientation θ and temperature T).

The reduced mobility may be determined from simulations without a triple junction—i.e., a bicrystal (see Fig. 1(b)). Following similar logic to that used in deriving Eq. (7), we obtain the grain boundary migration rate v_b to be

$$v_b = M_b \gamma \kappa = \frac{2M_b\gamma}{w}. \qquad (11)$$

Thus, in the bicrystal case, the rate of change of area $\dot{A}_b$ of the half-loop grain a is

$$\dot{A}_b = v_b w = 2M_b \gamma. \qquad (12)$$

Extracting $\dot{A}_b$ from the U-shaped half-loop simulations (see Fig. 1(b)), we obtain an independent measure of the reduced grain boundary mobility.

In order to put the magnitude of the triple junction mobility in perspective, we focus on the ratio of the triple junction mobility to that of the grain boundaries of the same misorientation. The dimensionless triple junction mobility Λ is

$$\Lambda = \left(\frac{M_{TJ} w}{M_b} \right). \qquad (13)$$

The width w in the numerator of Eq. (13) is included in the definition of Λ because the triple junction and grain boundary mobilities (Eqs. (2) and (7)) have different dimensionality: This may be traced to the fact the triple junction is of one lower spatial dimension than the grain boundaries. In the limit that $\Lambda \gg 1$, the triple junction mobility is very large and hence it has no influence on boundary migration (as discussed above). On the other hand, when this is not true, the triple junction can strongly modify the motion of the grain boundaries and the rate of change of grain a area may be significantly slower than expected based on the common $\Lambda = \infty$ assumption. Λ can be determined directly from the simulations by measuring $\dot{A}_{TJ}$ and $\dot{A}_b$. (see Fig. 1a and b). Inserting $\dot{A}_{TJ}$ and $\dot{A}_b$ from Eqs. (8) and (12), respectively (for the same T and θ) yields

$$\Lambda_{sim} = \frac{M_{TJ} w}{M_b} = \frac{\dot{A}_{TJ}}{\dot{A}_b} = \left(\frac{1}{\cos \beta_d - \cos \beta_s} \right) \quad (14)$$

where we have used the notation Λ_{sim} to indicate that this value is extracted entirely from simulation data ($\dot{A}_{TJ}$, $\dot{A}_b$, β_s and β_d). The mobility ratio can also be calculate directly from the analytical result for the triple junction migration (Eq. 10) in conjunction with Eq. (8):

$$\Lambda_{an} = \frac{M_{TJ} w}{M_b} = \frac{\beta_d}{\cos \beta_d - \cos \beta_s} \qquad (15)$$

where we have used the notation Λ_{an} to indicate that this value is extracted using the analytical relation for v_{TJ} of Galina et al. Λ_{an} is a function of the static and dynamic angles, β_s and β_d, only.

In this study, we extract the triple junction mobility for varying half-loop widths w and misorientation, θ. We first determine the dependence of the triple junction mobility on the half-loop width, to confirm the validity of the analytical results and to ensure that the range of w used in the simulations is sufficiently large. We extract the values of $\dot{A}_{TJ}$ and $\dot{A}_b$ and the static and dynamic

angles β_d and β_s from the simulation in order to determine the triple junction and boundary mobilities. These data are used to predict Λ using both Eqs. (14) and (15), in order to ensure that the two approaches yield consistent results. Finally, we investigate the misorientation dependence of θ and identify situations where the triple junction mobility is low enough to exert sufficient drag on boundary migration to significantly modify how boundaries migrate.

III. Simulation Method

The simulation results reported herein were performed in two-dimensions using the molecular dynamics simulation method and the a simple, empirical (Lennard-Jones) pair potential. The entire simulation cell, shown in Fig. 1, is constrained to lie entirely in the XY-plane. The lateral edges of the simulation cell are left free so as to decrease the effect of any stresses produced due to the initial as-constructed triple junction geometry and to allow the system to elastically remove the excess volume associated with the densification of the system when the total length of grain boundaries decrease. The top and the bottom layers are frozen in the horizontal direction (relative to Fig. 1) and allowed to relax along the vertical direction. The simulations were all performed at constant temperature T and the number of atoms in the computational cell, N, was fixed. The underlying crystal structure is a triangular lattice with a nearest neighbor spacing r_0. For more details on the MD simulation technique used in this study, see [14]. Energies are reported in units of the Lennard-Jones potential well depth ε, distance in units of the equilibrium atom separation r_0, area in units of the perfect crystal area per atom a_0 and times in units of $\tau = (M_{at} r_0^2 / \varepsilon)^{1/2}$, where M_{at} is the atomic mass.

The starting configuration used in the triple junction migration simulations (Fig. 1(a)) is a half-loop shaped grain boundary geometry (see Fig. 1(b)), with an additional straight grain boundary at the apex of the half-loop and parallel to the sides of the half-loop, as shown explicitly in Fig. 2. As mentioned before, the grains b_1 and b_2 and are misoriented with respect to grain a by θ and are equivalent to each other. The initially straight $b_1 b_2$ grain boundary separates grains misoriented from each other by 2θ. This entire as-constructed triple junction geometry is then allowed to relax at a very low temperatures (0.010–$0.025\,\varepsilon/k$), prior to the grain boundary migration study in order to enable the atoms at the grain boundaries to equilibrate.
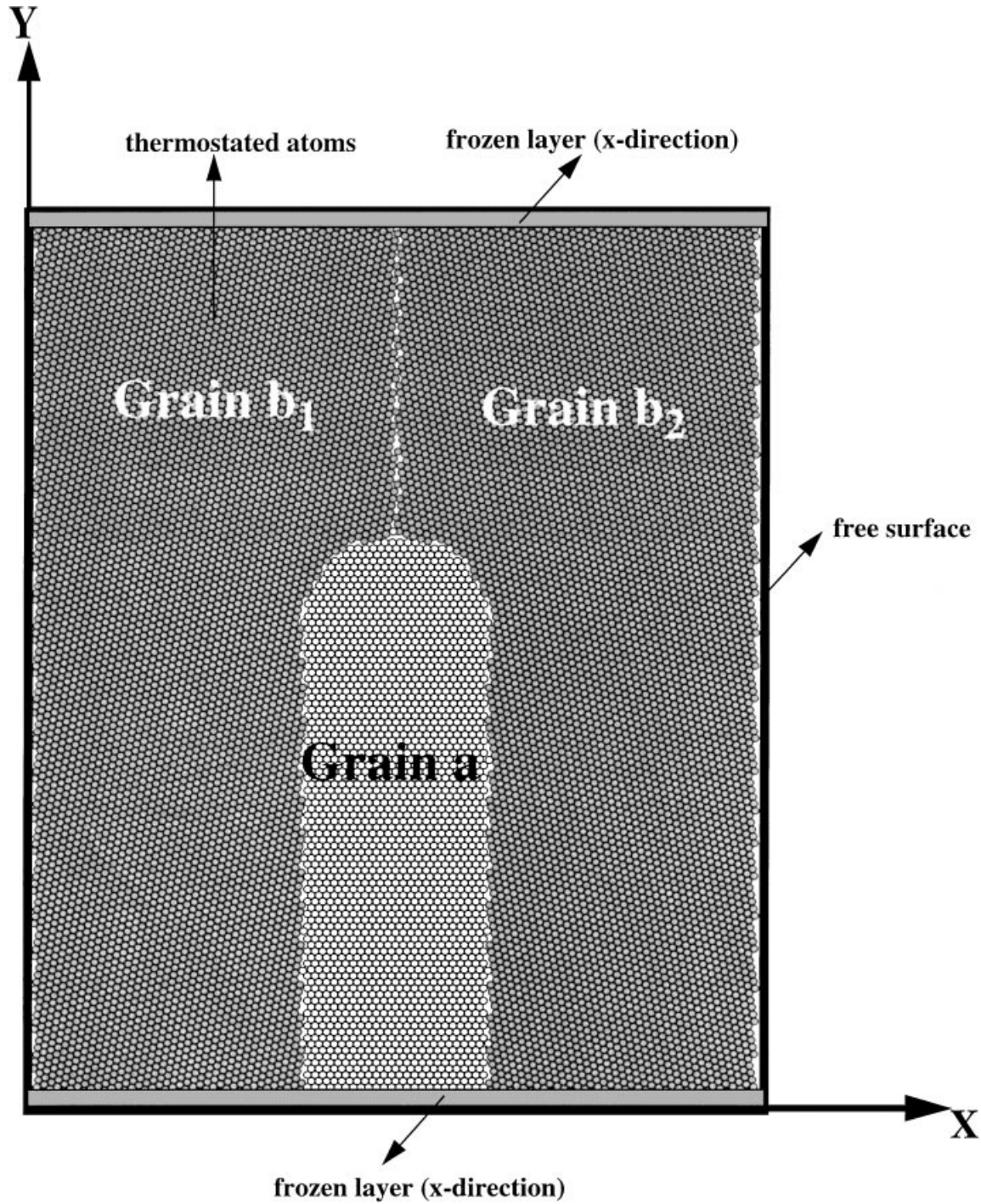
Figure 2. The actual simulation cell showing the initial as-constructed configuration of the triple junction for a $\Sigma 7$ ($\theta = 38.2°$) misorientation across the boundary.
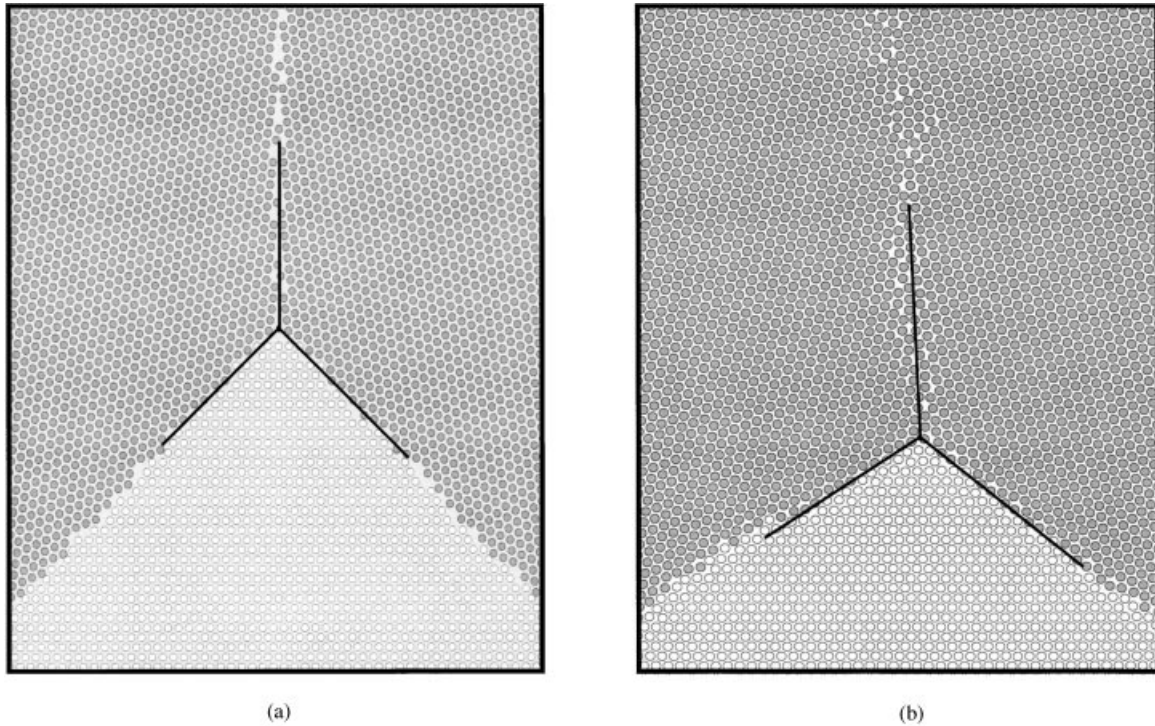
(a)

(b)

Figure 3. The (a) initial and (b) final atomic configurations in a molecular dynamics simulation designed to determine the equilibrium static triple-junction angle β_s.

The entire system is slowly raised to the desired temperature in a step-wise fashion and the migration rate ($\dot{A}_{TJ}$) is deduced by from the slope of an A_{TJ} versus time plot. A_{TJ} is simply the number of atoms in grain a times the area per atom a_0 ($=3\sqrt{3}r_0^2/8$). This requires the assignment of each atom in the simulation cell to one of the grains at each time, as described in detail in [14]. Care is taken to ensure that the slopes of A_{TJ} versus time are extracted only when the migration is occurring with a self-similar shape. The extraction of dynamic triple junction angle β_d is carried out by measuring the opening angle at the apex of grain a (i.e., $\beta_{ab_1} + \beta_{ab_2} = 2\beta_d$, see Fig. 1(a)). This is accomplished by measuring the angle enclosed by tangent vectors to the ab_1 and ab_2 boundaries at the apex of grain a. β_d measurements are only made during times for which grain a is retracting in a self-similar manner. The average over these angle measurements is reported.

The static equilibrium angle β_s, (see Eq. (5)) is determined using the starting simulation cell geometry shown in Fig. 3(a). At the beginning of the simulation, the angle β is set at 45° but evolves during the MD simulation run at the desired temperature. The grain boundaries migrate until the equilibrium angle is established and all boundaries are flat (Fig. 3(b)). Measurement of this angle yields β_s. β_s is determined in this manner for all values of θ for which triple junction mobility is measured at the temperature of interest.

In order to measure the triple junction mobility in the smallest possible simulation cell, we performed a series of simulations with different half-loop widths w (Fig. 1) to ascertain the minimum width for which the triple junction mobility is independent of width. This is necessary because if w is too small, elastic interactions between different boundary segments may modify the driving force for boundary migration and the boundary migration mechanism may be constrained. These simulations were performed for a misorientation of $\theta = 38.2°$ at $T = 0.125\,\varepsilon/k$ for half-loops with widths $19r_0 \leq w \leq 29r_0$. The results are discussed below.

The dependence of triple junction mobility on grain boundary and triple junction crystallography is simulated in tricrystals for a range of boundary misorientations (the misorientations across the ab_1 and ab_2 is θ and across b_1b_2 is 2θ). Special or singular boundaries (e.g.,

$\Sigma = 7, \theta = 38.2°$ and $\Sigma = 13, \theta = 32.21°$ where Σ is the inverse density of coincident sites) vicinal or near singular boundaries (near $\Sigma = 7$ and $\Sigma = 13$) and general boundaries were all simulated. It should be noted that in the present 2-d triangular lattice simulations, where misorientations correspond to tilts about the $\langle 111 \rangle$ axis in the fcc lattice, a value of Σ across the ab_1 and ab_2 (θ) grain boundaries leads to a Σ value for the b_1b_2 boundary equal to the square of that for the ab_1 or ab_2 boundaries. All misorientations were within the range $30° \leq \theta \leq 40°$, where the entire range of unique boundary misorientations lies between $30° < \theta < 60°$. All of the simulations reported herein were performed for $T = 0.125 \, \varepsilon/k$ and the data reported corresponds to averages over at least three simulation runs.

IV. Half-Loop Profile

The atomic configuration of the retracting triple junction half-loop is shown in Fig. 4(a) and (b) at two different times ($t = 320 \, \tau$ and $2550 \, \tau$), for a simulation performed at $T = 0.125 \, \varepsilon/k$, with an ab_1 and ab_2 misorientation of $\theta = 33.5°$ (i.e., a high Σ boundary near $\Sigma 13$) and a half-loop width of $w = 25 \, r_0$. This figure demonstrates that apart from small fluctuations, the half-loop shape is very nearly self-similar and that the triple junction angle is preserved during steady-state half-loop retraction/triple junction migration. Figure 5(a) and (b) show the results of a triple junction migration simulation under the same conditions as Fig. 4, but for ab_1 and ab_2 boundary misorientations of $\theta = 38.2°$, at $t = 450 \, \tau$ and $2550 \, \tau$, respectively. This angle corresponds to a high symmetry, $\Sigma 7$, misorientation. In this case too, the half-loop triple junction retraction takes place in a nearly self-similar fashion. We commonly observe self-similar triple junction, half-loop profiles during migration for all misorientations.

The dynamic triple junction angle β_d is measured at several times during the half-loop retraction by measuring the enclosed angle between the two tangent vectors to the sides of the half-loop at the triple junction. For the simulations depicted in Fig. 4, $\theta = 33.5°$ (high Σ),

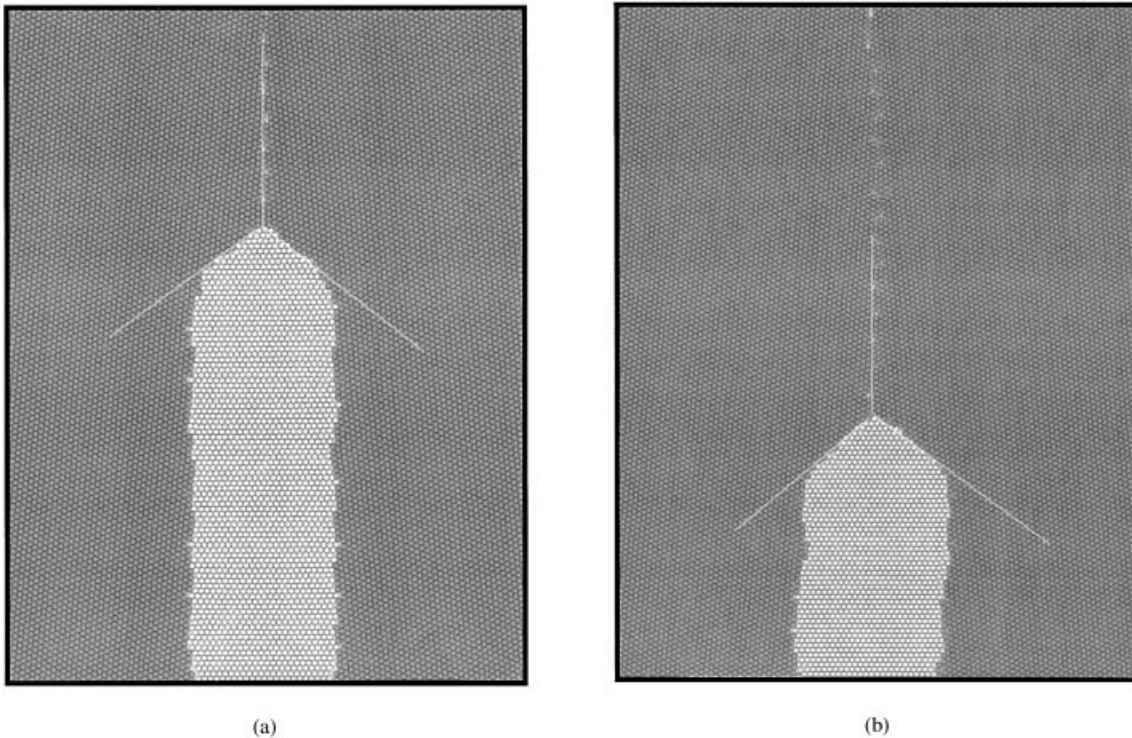(a)   (b)

Figure 4.   The atomic configurations of a $\theta = 33.5°$ migrating triple junction ($T = 0.125 \, \varepsilon/k$, $w = 25r_0$) at two instants of time: (a) $t = 320 \, \tau$ and (b) $2550 \, \tau$. The white lines indicate the tangents to the half-loop boundary at the triple junction. The dynamic triple junction angle was $56°$ in (a) and was $58°$ in (b).
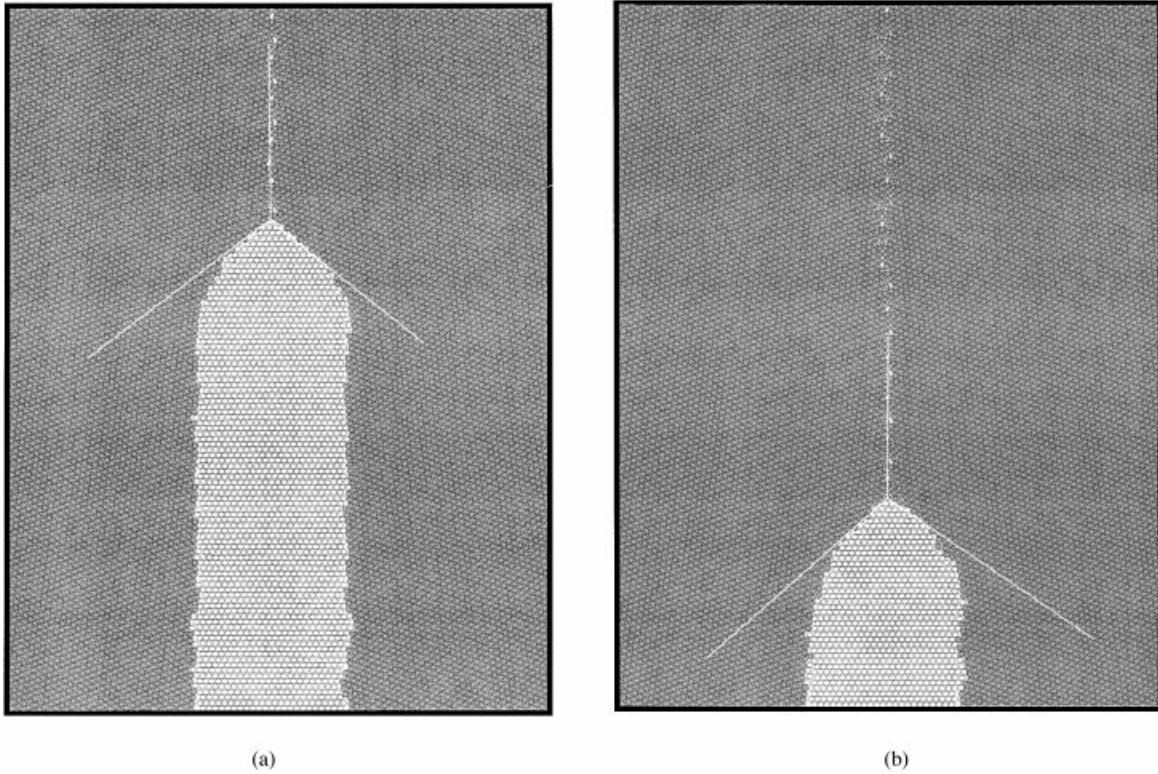
Figure 5. The atomic configurations of a $\theta = 38.2°$ ($\Sigma = 7$) migrating triple junction ($T = 0.125\,\varepsilon/k$, $w = 25r_0$) at two instants of time: (a) $t = 450\,\tau$ and (b) $2150\,\tau$. The white line indicate the tangents to the half-loop boundary at the triple junction. The dynamic triple junction angle was $47°$ in (a) and was $48°$ in (b).

the dynamic triple junction angle is measured to be $\beta_d = 56° \pm 1°$ (the uncertainty is associated with fluctuations in half-loop shape and in measurement). For the low Σ boundary ($\Sigma 7$, $\theta = 38.2°$) shown in Fig. 5, the dynamic triple junction angle β_d is $47 \pm 1°$. For both these boundaries the static triple junction angle is while the static angle β_s is $60 \pm 1°$.

A series triple junction, half-loop migration simulations were performed for 13 different grain boundary misorientations at fixed width ($w = 25r_0$) and for five widths at fixed misorientation ($\theta = 38.2°$) at $T = 0.125\,\varepsilon/k$. The dynamic triple junction angle is tabulated in Table 1 as a function of half-loop width w. The dynamic triple junction angle is seen to be relatively insensitive to variations in half-loop width. This suggests that the dynamic triple junction angle is determined locally, rather than by interactions that are substantially longer range than atomic dimensions (not so for its migration rate, as discussed below).

The variation of the dynamic angle β_d with ab_1 and ab_2 boundary misorientation θ is shown in Table 2.

Also shown in Table 2 is the boundary misorientation dependence of the static triple junction angle β_s. The static triple junction angles are nearly independent of misorientation in this two-dimensional, Lennard-Jones simulation and are very close to the isotropic limit of $\beta_s = 60°$. On the other hand, the dynamic triple junction β_d varies from a low of $44° \pm 1°$ to a high of

Table 1. The values of the rate of change of area $\dot{A}_{TJ}$ of the half-loop grain and the dynamic triple junction angle β_d as a function of the half-loop width w for the triple junction with grain boundary ab misorientation $\theta = 38.2°$ ($\Sigma = 7$).

Width $w(r_0)$	$\dot{A}_{TJ}(a_0/\tau)$	β_d (°)
19	1.23 ± 0.2	47 ± 1
21	1.02 ± 0.2	46 ± 1
23	0.33 ± 0.1	47 ± 1
25	0.52 ± 0.2	46 ± 1
29	0.51 ± 0.1	47 ± 1

Table 2. The tabulated values of the extracted rate of change of area of the half-loop grain $\dot{A}_b$ (extracted from bi-crystal simulations [13]), the rate of change of area grain a during the triple junction migration $\dot{A}_{TJ}$ and the dynamic and statiac triple junction angle β_d and β_s and the calculated values of Λ_{sim} and Λ_{an} as a function of the grain boundary ab misorientations θ.

θ (°)	$\dot{A}_b(a_0/\tau)$	$\dot{A}_{TJ}(a_0/\tau)$	β_d (°)	β_s (°)	Λ_{sim}	Λ_{an}
31.50	0.51 ± 0.02	0.49 ± 0.02	59 ± 1	60 ± 1	63.90	68.47
32.00	0.45 ± 0.02	0.31 ± 0.04	57 ± 1	60 ± 1	15.43	22.28
32.21	0.37 ± 0.02	0.13 ± 0.02	44 ± 1	60 ± 1	1.60	3.50
33.00	0.38 ± 0.03	0.25 ± 0.03	53 ± 1	60 ± 1	6.46	9.08
33.57	0.49 ± 0.05	0.47 ± 0.05	56 ± 1	60 ± 1	16.20	16.51
34.00	0.41 ± 0.01	0.41 ± 0.01	59 ± 1	61 ± 1	34.25	34.06
35.57	0.52 ± 0.05	0.48 ± 0.05	58 ± 1	60 ± 1	30.85	33.83
37.00	0.71 ± 0.02	0.74 ± 0.02	59 ± 1	60 ± 1	63.80	68.47
37.52	0.89 ± 0.03	0.55 ± 0.03	54 ± 1	60 ± 1	7.04	10.74
38.22	1.57 ± 0.01	0.41 ± 0.01	47 ± 1	60 ± 1	1.43	4.51
38.98	0.98 ± 0.04	0.57 ± 0.04	50 ± 1	61 ± 1	3.68	5.52
39.50	0.72 ± 0.03	0.69 ± 0.03	59 ± 1	62 ± 1	21.03	22.60
39.92	0.53 ± 0.04	0.55 ± 0.04	59 ± 1	60 ± 1	69.00	68.47

$59° \pm 1°$. Dynamic triple junction angles near (within the error bars of) the static value of $60°$ are well represented in the simulation performed, while low values of β_d are rare. Low values of β_d occur only at or very near low Σ misorientations: $\beta_d = 44°$ for $\Sigma 13$ ($\theta = 32.2°$) and $\beta_d = 47°$ for $\Sigma 7$ ($\theta = 28.2$).

V. Migration Kinetics

As described above, the time dependence of the area of grain a, $A_{TJ}(t)$, is determined by counting the number of atoms in grain a at each instant of time. The temporal evolution of the area of grain a A_{TJ} is shown in Fig. 7(a) for the same conditions as in Fig. 4: namely, $\theta = 33.5°$ (i.e., a high Σ boundary near $\Sigma 13$), $T = 0.125 \, \varepsilon/k$, and a half-loop width of $w = 25r_0$. The half-loop area decreases with time in a monotonic fashion, with some superimposed noise. At late times, the retracting half-loop is influenced by the frozen layer of atoms at the bottom of the simulation cell and, hence, no reliable measurements of $\dot{A}_{TJ}$ can be made there. Some of the fluctuations seen in Fig. 7(a) at intermediate time are associated with thermal transients in the shape of the half-loop and triple junction angle during half-loop retraction. These transients are excluded during the determination of the steady-state slope of the curve, $\dot{A}_{TJ}$. Also shown in the same plot (Fig. 7(a)) is simulation data obtained

for the bicrystal half-loop (i.e., without a triple junction) simulation (see Fig. 1(b)), A_b vs. t, for the same misorientation, temperature and half-loop width as for the triple junction migration simulation. The slope of this curve, indicated by the linear curve fit, is $\dot{A}_b$. As for the triple junction migration simulation, the slope $\dot{A}_{TJ}$ is extracted only in the steady-state regimes. More detailed discussion of the nature of the fluctuations in the A vs. t plots may be found elsewhere [15]. Note that for the simulation with $\theta = 33.5°$, the two curves in Fig. 7(a) have similar slope, i.e. $\dot{A}_{TJ} \approx \dot{A}_b$.

Similar data is presented in Fig. 7(b) for the case shown in Fig. 5—$\theta = 38.2°$ ($\Sigma 7$), $T = 0.125 \, \varepsilon/k$, and a half-loop width of $w = 25r_0$. Unlike for the low symmetry $\theta = 33.5°$ case, the steady-state slopes of the A vs. t plots for the half-loops with and without the triple junction are substantially different. The half-loop with the triple junction moves much more slowly than that with no triple junction for $\theta = 38.5°$. This implies that the at least for the $\theta = 38.5°$ case, triple junction drag may be substantial. These results parallel the observation that the dynamic and static triple junction angles are very similar for $\theta = 33.5°$ and substantially different for $\theta = 38.5°$. Together, these data suggest that there may be a correlation between the deviation of the dynamic triple junction angle from its static value and triple junction drag.

The values of the steady-state, triple junction, half-loop $\dot{A}_{TJ}$ were measured for 13 different grain boundary misorientations at fixed width ($w = 25r_0$) and for five widths at fixed misorientation ($\theta = 38.2°$) at $T = 0.125 \, \varepsilon/k$. This data was analyzed to determine the triple junction migration rate $v_{TJ} = \dot{A}_{TJ}/w$. Table 1 shows the extracted values of $\dot{A}_{TJ}$ and β_d as a function of half-loop width, w at a fixed misorientation, $\theta = 38.2°$. The calculated values of v_{TJ} are plotted as a function of the inverse half-loop width w in Fig. 6. For sufficiently large values of the half-loop width, the triple junction velocity is inversely proportional to w—consistent with the prediction of Eq. (9). At small w, substantial deviations from this relationship is observed and hence not viewed as reliable for determining migration rates (as discussed in [14]). The deviation of the small width data from the predicted behavior is most likely associated with elastic interactions between different segments of the grain boundary not included in the derivation of the driving force for curvature driven grain boundary migration. These data are in distinction to the dynamic triple junction angle, which was relatively insensitive to variations in half-loop width.
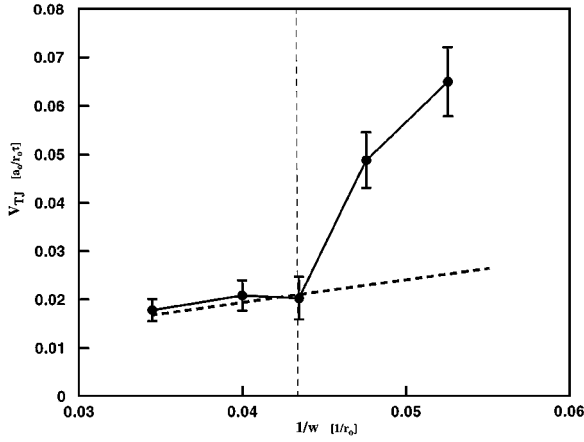
Figure 6. The migration rate of the triple junction, v_{TJ}, plotted as a function of the inverse of half-loop width, w for $T = 0.125\,\varepsilon/k$ and $\theta = 38.2°$, $\Sigma = 7$.

The values of $\dot{A}_{TJ}$ obtained from the steady state regions of plots of the same type as in Fig. 7 are tabulated as a function of the ab_1 and ab_2 grain boundary misorientation θ in Table 2, along with the rate of change of area of a bicrystal half-loop grain $\dot{A}_b$. Depending on the misorientation, $\dot{A}_{TJ}$ and $\dot{A}_b$ can be very similar (within the error bars) or very different (by a factor as large as nearly four). The difference between $\dot{A}_{TJ}$ and $\dot{A}_b$ is largest for the low Σ (singular) boundaries examined. As described above, the difference between the dynamic and static β_s triple junction angles (β_d and β_s, respectively) discussed above is also greatest for low

Σ boundaries. These observations provide additional support to the notion, discussed above, that there is a correlation between the deviation of the dynamic triple junction angle from its static value and triple junction drag on grain boundary migration.

VI. Triple Junction Mobility

The triple junction mobility can be derived from the rate of change of area of the triple junction half-loop grain, as per Eq. (8). Instead of focusing on the triple junction mobility itself, it is more appropriate to examine the triple junction mobility relative to the mobility of the grain boundaries it bounds. The appropriate dimensionless ratio Λ is $\Lambda = (M_{TJ}\,w)/M_b$. We determined Λ from the simulations using two distinct approaches: by directly measuring $\dot{A}_{TJ}$, $\dot{A}_b$, β_d, and β_s from simulations Λ_{sim} (see Eq. (14)) and by a combination of the analytical results of Galina et al. [11] and simulation results Λ_{an} (see Eq. (15)).

Using the $\dot{A}_{TJ}$, $\dot{A}_b$, β_d, and β_s data contained in Table 2, we determine Λ_{sim} and Λ_{an} and collect the results in Table 2 as a function of grain boundary misorientation. The variation of these two parameters with the ab_1 and ab_2 grain boundary misorientation angle θ is shown in Fig. 8. The two measures of Λ are nearly indistinguishable. This demonstrates the equivalence of the two approaches for determining Λ (Eqs. (14) and (15)) and proves that $\dot{A}_{TJ}/\dot{A}_b = \beta_d$. The presence of only a very small deviation between Λ_{sim} and
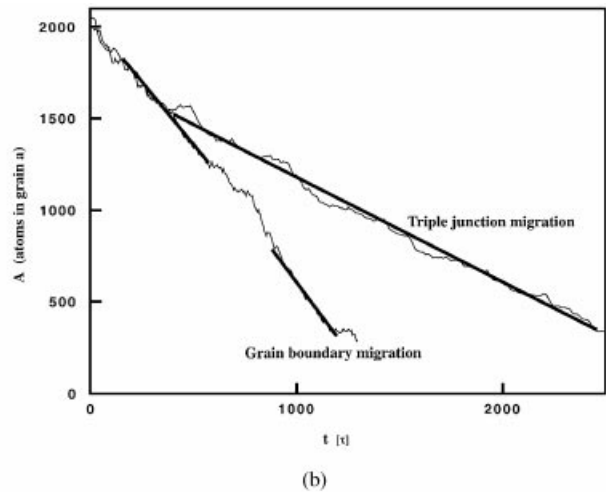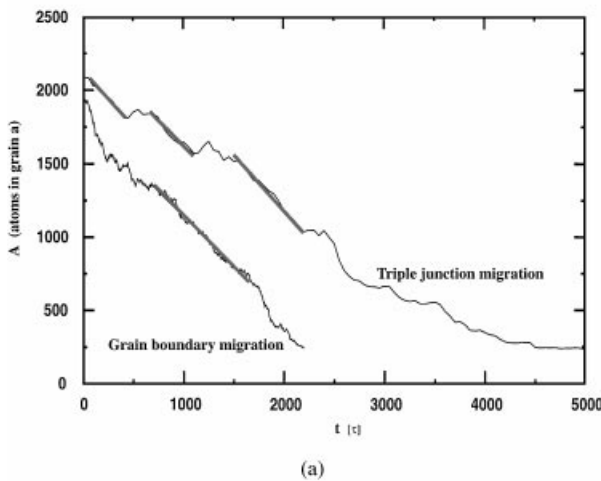

Figure 7. The rate of change in the area of the half-loop grain (grain a) for the triple junction and bicrystal geometries at $T = 0.125\,\varepsilon/k$ and $w = 25\,r_0$ for (a) $\theta = 33.5°$ and (b) $\theta = 38.2°$.
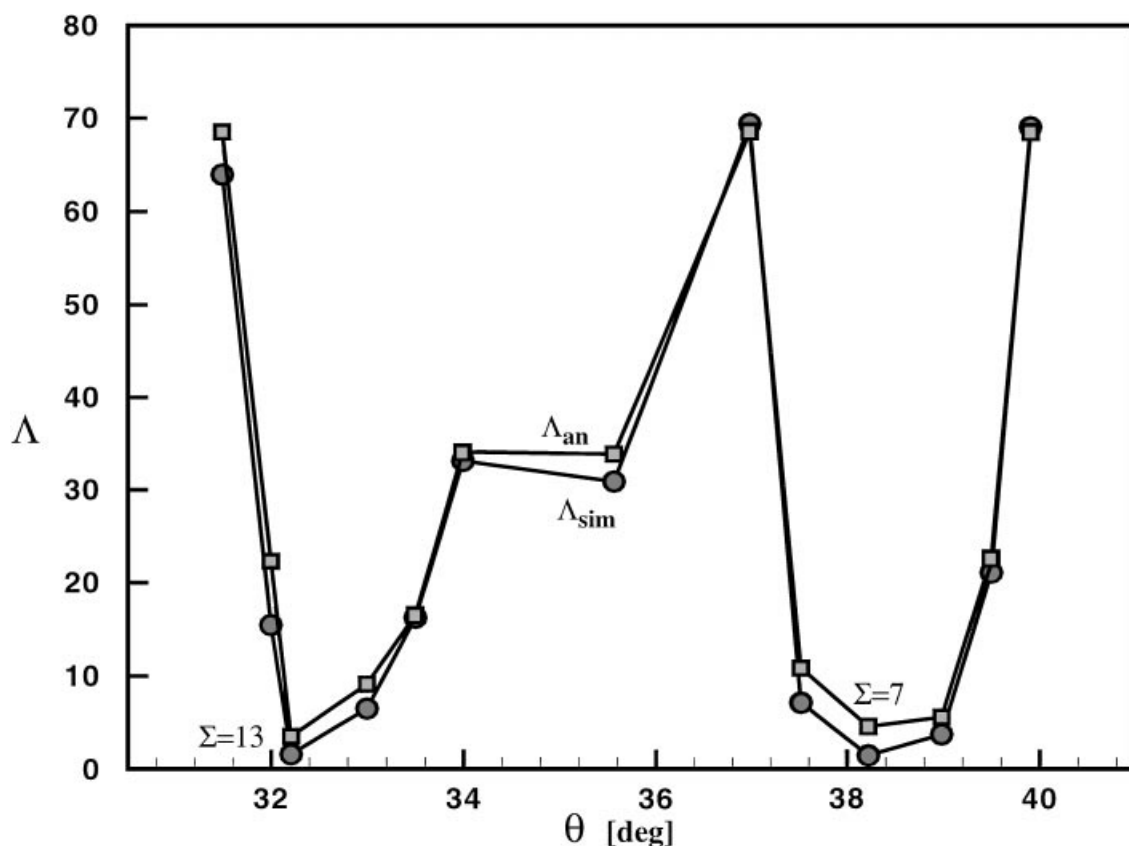
Figure 8. The dimensionless triple junction mobility parameter, $\Lambda = (M_{TJ}w)/M_b$, plotted as a function of the grain boundary misorientation θ for $w = 25\,r_0$ and for $T = 0.125\,\varepsilon/k$.

Λ_{an} also shows that the values of $\dot{A}_{TJ}$, $\dot{A}_b$, β_d, and β_s extracted from two distinct types of simulations are reliable.

The variation of Λ with misorientation shown in Fig. 8 is not monotonic, but rather exhibits distinct maxima and minima. Because of the finite angular resolution in the data, it is not possible to determine whether the minima in Λ that occur at the $\Sigma 7\,(\theta = 38.2°)$ and $\Sigma 13\,(\theta = 32.2°)$ boundaries\are indeed cusps as occur in plots of grain boundary energy vs. misorientation. Nonetheless, it is clear that the low Σ misorientations are indeed special. Since the values of Λ a which these minima occur are of order unity (i.e., Λ is not much greater than one), these triple junctions clearly exert considerable drag on the grain boundaries in the present simulations.

The dimensionless triple junction mobility Λ is proportional to the half-loop width w. Since w is very small in the present simulation ($w = 25r_0$), the effect of triple junction drag is significant for certain misorientations.

If, on the other hand, the width of the half-loops were of the scale of grain sizes in typical polycrystalline materials, Λ would be much greater than one for all boundaries and triple junction drag would have little effect on grain growth kinetics. Triple junction drag may be significant even at larger grain sizes if solute or impurities are present (even at extremely low concentrations) because of preferential segregation to triple junctions and the drag caused by pulling along the triple junction solute cloud. Even without impurities, triple junction drag may be important in thin films and other nanocrystalline materials, where the characteristic grain size is inherently very small.

Acknowledgments

References

1. G. Palumbo, D.M. Doyle, A.M. El Sherik, U. Erb, and K.T. Aust, Scripta Metall. Mater. **25**(3), 679 (1991).
2. E. Ho and G.C. Weatherly, Acta Metall. **23**(12), 1451 (1975).
3. M.H. Yoo and H. Trinkaus, Metall. Trans. A **14A**(4), 547 (1983).
4. G. Palumbo and K.T. Aust, Mat. Sci. Eng. A **A113**(1), 139 (1989).
5. S. Hashimoto, T.K. Fujii, and S. Miura, Scripta Metall. **21**, 169 (1987).
6. A.H. King, Materials Science Forum **294–296**, 91 (1999).
7. S.G. Srinivasan, G. Kalonji, and R.W. Cahn, private communication.
8. W.W. Mullins, Journal of Applied Physics **27**(8), 900–904 (1956).
9. V.N. Perevezentsev and M.Y. Shcherban, Sov. Phys. Solid State **5**, 36 (1982).
10. C.V. Kopetskii and L.K. Fionova, Sov. Phys. Solid State **12**, 111 (1982).
11. A.V. Galina, V. Ye. Fradkov, and L.S. Shvindlerman, Phys. Met. Metall. **36**(6), 165 (1987).
12. U. Czubayko, V.G. Sursaeva, G. Gottstein, and L.S. Shvindlerman, Acta Mater **46**(16), 5863 (1998).
13. A.S. Lazarenko, I.M. Mikhailovskij, V.B. Rabukhin, and O.A. Velikodnaya, Acta Metall. Mater. **43**(2), 639 (1995).
14. M. Upmanyu, R.W. Smith, and D.J. Srolovitz, Interface Science **6**, 41 (1998).
15. M. Upmanyu, D.J. Srolovitz, L.S. Shvindlerman, and G. Gottstein, Interface Science **6**, 257 (1998).